An overview of methods for handling, and issues facing, subgrid-scale radiative transfer in large-scale atmospheric models

Howard W. Barker

Meteorological Service of Canada
Cloud Physics Research Division (ARMP), 4905 Dufferin St.,
Downsview, ON, Canada M3H 5T4

1. Introduction

It would not be too difficult to argue that the essence of Earth's climate stems from the 4D interaction between radiation and the three phases of water. Perturbations to Earth's radiation budget form the impetus for climatic change and the response of the system to a radiative perturbation is in turn governed much by radiative feedbacks. Moreover, the most comprehensive means of assessing climate and climatic change is through radiometric measurements made on satellites. Currently, much research on Large-scale Atmospheric Models (LSAMs) involves developing and testing parametrizations of subgrid-scale processes, and radiation is no exception. Radiation is, however, somewhat special, not only because of its central role in climate and climate studies, but also because subgrid-scale issues are encountered in both unresolved spatial scales, and spectral space too. As such, radiative transfer and optical fluctuations must be parametrized at unresolved spatial scales, while sweeping averages over wide spectral intervals are required too.

Radiation as a subgrid-scale problem for LSAMs is addressed in this lecture series in two parts. The first part, housed in this chapter, deals with mainstream aspects such as gaseous transmittance, surface properties, cloud optical properties, and1D radiative transfer modelling. The second part discusses issues facing parametrization of radiative transfer for 3D cloudy atmospheres; this includes both modelling in LSAMs and remote sensing.

Thus, the outline of this chapter is as follows. The second part touches on the state of parametrization of some optical properties. This is viewed as separate from radiative transfer which is dealt with in the third section. A lengthier discussion of parametrizing interactions between unresolved fluctuations and radiative transfer is deferred to the other chapter. Conclusions are given in the fourth section.

2. Parametrization of optical properties

For practical purposes, it is assumed that the only source of radiant energy to Earth is from the Sun at wavelengths λ between ~0.2 μm and ~5 μm and that emission of terrestrial infrared (IR) radiation is confined to λ between ~5 μm and ~50 μm. While there is some overlap between these sources, it is fairly minor and is usually neglected (e.g., Liou 1992). Typically, an LSAM resolves the solar spectrum into between 2 to 10 bands and the IR spectrum into 5 to 20 bands. Hence, much spectral information is unresolved thereby making rapid and accurate parametrizations of transmittance (and optical properties) essential. As such, this section has four main parts that contain discussion of parametrization of optical properties for: 1) gases; 2) aerosols; 3) surfaces; and 4) clouds.

2.1 Gaseous transmittances

If it were computationally feasible, radiative transfer through gases would be computed using extremely high spectral resolution line-by-line (LBL) simulations (e.g., Ramaswamy and Freidenreich 1991; Clough et al. 1989). These models are based on detailed descriptions of spectral lines in conjunction with assumptions about line structure and interactions. Generally, broadening of lines are assumed to be a certain shape and to extend for about 25 cm^{-1} either side of line centre. The computational burden of LBLs, however, (even for cloudless-sky conditions) restricts them to be purveyors of valuable high spectral resolution benchmarks for well-defined atmospheres that can be used to assess other, more approximate, models.

In an LSAM one can expect to execute only a relatively small number of multi-layer radiative transfer simulations for each atmospheric column. This renders LBL calculations out of the question. As a result, sweeping integrations over broad spectral bands must be done where representative optical properties are used in a radiative transfer algorithm designed for monochromatic radiation.

Several methods exist for computing broadband transmittances for gaseous atmospheres (e.g., Fouquart and Bonnel 1980; Wiscombe and Evans 1976). It is probably safe, however, to assume that operational, broadband (BB) atmospheric radiative transfer modelling is firmly entrenched in the correlated-k distribution (CKD) paradigm (Lacis et al. 1979; Lacis and Oinas 1991); the essence of which rests in its parent k-distribution method (Arking and Grossman 1972). The utility of the k-distribution method can be appreciated by considering transmittance averaged over a spectral interval $\Delta\nu$ (for uniform spectral irradiance) along a straight line between two levels z_1 and z_2. An LBL model would compute it as

$$T_j = \int_{\Delta\nu} \exp\left[-\int_{z_1}^{z_2} k(\nu, p, T)\,\rho dz'\right] \frac{d\nu}{\Delta\nu} \tag{1}$$

where k is extinction coefficient, ν is wavenumber, ρ is density, p is pressure, and T is temperature. Likewise, if g denotes the cumulative frequency of k over $\Delta\nu$, the k-distribution method would compute transmittance as

$$T_j = \int_0^1 \exp\left[-\int_{z_1}^{z_2} k(g, p, T)\,\rho dz'\right] dg\,. \tag{2}$$

Figure 1 shows k across the O_2 A-band at two altitudes. On the left is k as a function of ν. Exponentiating this tortuous curve and computing the area under it is what an LBL model would do. On the right is k as a function of g. Clearly one could approximate transmittance well by judiciously choosing a relatively small number of Gaussian quadrature points; this is the attraction of the k-distribution method. The CKD method builds on the k-distribution method by harvesting obvious strong correlations between spectral signatures for different atmospheric states (see Fig. 1). For practical issues involving spectral-weighting and overlap of different gases, see Fu and Liou (1992).

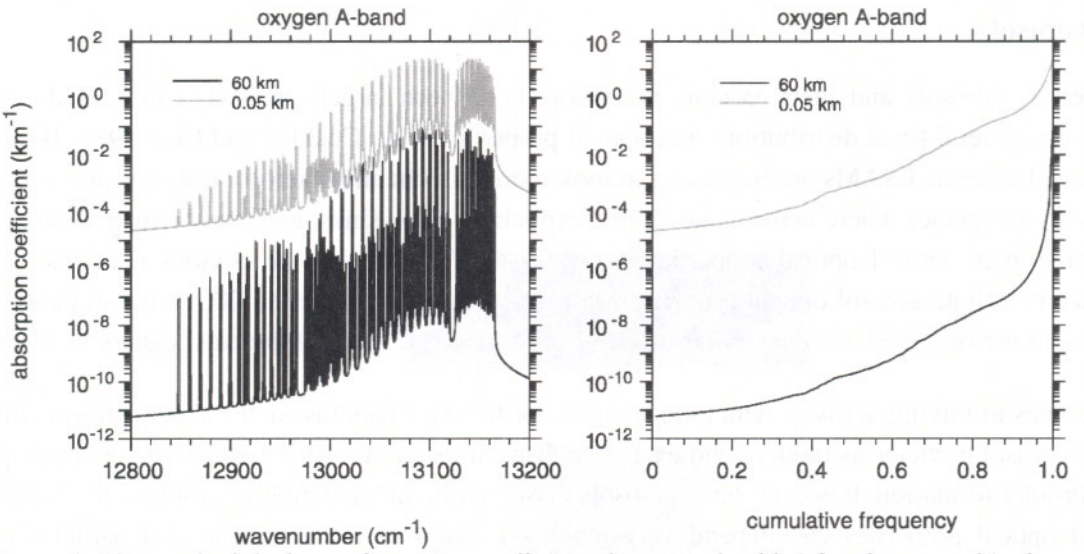

Figure 1. Plot on the left shows absorption coefficients k across the O2 A-band at two altitudes as functions of wavenumber ν. Plot on the right shows normalized cumulative distributions for the same k as plotted on the left.

An issue that has dogged IR radiative transfer for several years is that of the H2O vapour continuum. This is defined as any observed absorption due to H2O vapour not attributable to the Lorentz line contribution within 25 cm-1 of each line (Mlawer et al. 1999). It appears now that the lion's share of the H2O vapour continuum are the intermediate and far wings of allowed transitions of the H2O monomer plus collision-induced transitions of the H2O monomer. There are, however, minor contribution from dimers etc. Figure 2 shows an example of the extent to which a current representation of the H2O continuum brings model results into line with measurements.

Similarly, there is an H_2O continuum across the solar spectrum. It has been suspected for some time (e.g., Stephens and Tsay 1990) that this continuum may be partially responsible for some absorption anomalies for cloudy atmospheres. Currently the solar H_2O continuum is thought to contribute less than 3 W m-2 to atmospheric absorption averaged over the globe (per. comm., E. Mlawer 2001).

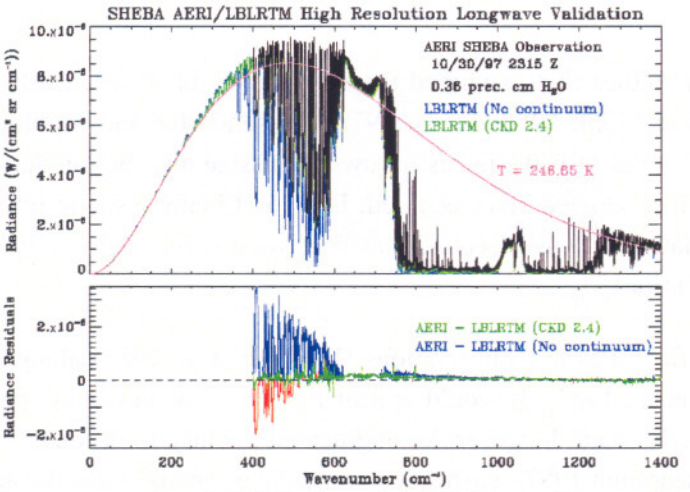

Figure 2. Top plot shows measured and modelled spectral LW downwelling radiances obtained at a high Arctic site. Bottom plot shows differences between measured and modelled radiances with and without a water vapour continuum. (Data courtesy of E. Mlawer 2001).

2.2 Aerosols

Until recently, aerosols and their gaseous precursors have been largely neglected in LSAMs, or at best ascribed very general fixed distributions and optical properties (e.g., Coakley and Cess 1985; Barker and Li 1995). Now, however, LSAMs are beginning to look more like chemical/aerosol transport models with their rich diversity of species where aerosols now have explicit sources, sinks, and transformation processes. Yet still, generation of aerosol optical properties is rather vague. There are the obvious relations such as the dependence of sulfate aerosol optical properties on relative humidity (Li et al. 2001), but in many instances when aerosols are observed, for example from cities or forest fires, much of the mass cannot be identified.

When it comes to mixing aerosols with clouds, most opt for the Chandrasekhar mean approach which treats cloud and aerosol particles as random and exclusive distributions (e.g., Blanchet 1982). The basic principles of cloud droplet formation, however, have aerosols dissolved in and adhering to droplets. It has been shown that cloud optical properties can depend very much on how one introduces aerosol particles into them (Chylek et al. 1978).

Since fluxes are of prime concern to LSAMs, the details of aerosol scattering phase functions are not necessary. If solar radiative transfer for aerosolized atmospheres is computed using a two-stream method that utilizes explicit integrals over particle phase functions (e.g., Coakley and Chylek 1975), either the Henyey-Greenstein (1941) or the elliptical phase function (Barker 1995) can be used to approximate more exact Mie calculations. Increasingly, however, this has become a moot point as most LSAMs use solutions to the radiative transfer equation that employ phase functions approximated by a sharp forward scattering peak (see Section 3.1.1). As such, all that is required is aerosol extinction coefficient, single-scattering albedo ω_0 and asymmetry parameter g (the mean cosine of scattering angle).

2.3 Surface albedo

The chief concern regarding optical properties of surfaces is their albedo across the solar spectrum. The two fundamental surface types, water and land, have dramatically different reflection properties. Some issues facing prescription of albedo for these broad classes are discussed here.

2.3.1 Water

There have been several studies that examined the dependence of water albedo on solar zenith angle and wind speed (e.g., Cox and Munk 1956; Payne 1972; Priesendorfer and Mobley 1986). Cox and Munk's method assumes that the slopes of wave facets follow a Gaussian distribution that depends on wind speed $|\mathbf{v}|$ and that only Fresnel reflection need be considered. Despite it being a single-reflection model that does not account for spatial correlation of wave facets, it has been used successfully to infer $|\mathbf{v}|$ from observations of sun glint (its original intention).

Figure 3 shows a curve fit to Payne's observations (Briegleb et al. 1986) along with results from Cox and Munk's model (Hansen et al. 1983). It would appear that the Cox and Munk parametrization captures the essence of ocean albedo. It could, however, be augmented slightly to account for the effects of whitecaps (Monahan and O'Muircheartaigh 1987), suspended particulates, and bottoms (in shallow areas).

2.3.2 *Land*

Most LSAMs employ land surface type databases to prescribe surface albedo. Basically, each surface type (e.g., soil, as well as primary and secondary vegetation types) gets assigned an albedo, which usually does not (but should) depend on cosine of solar zenith angle μ_0, and a mean albedo is created for each cell by weighting each sub-albedo by its fractional area. This value is then used as the lower boundary condition of the atmospheric radiative transfer model. For many surface types this is probably adequate. In fact, a common practice is to compute mean surface irradiance using a single surface albedo, but then allow for variable absorption of radiation by different surface types using their respective albedo. This enables a surface energy budget to be maintained for different subgrid surface types. This is essential for cells containing snow, ice, or water in conjunction with bare land.

As representations of the biosphere in LSAMs become more sophisticated (cf., ESA's proposed SPRECTA satellite mission; ESA 2001), it may become necessary to account for detailed and complex radiative transfer within vegetation canopies (primarily forests and grasses). This would allow for vertical profiles of photosynthetically active radiation inside canopies.

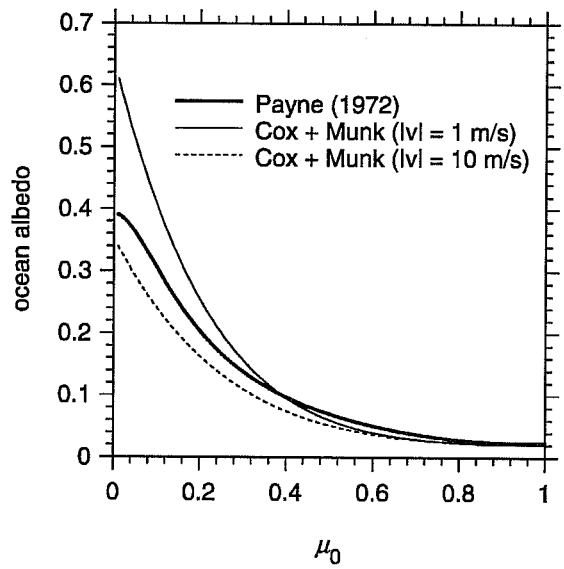

Figure 3. Heavy solid line shows a curve fit to observed ocean albedo. Other lines are predictions by the Cox and Munk wave slope approach for two wind speeds.

Additionally, there are certain biases that emerge when dealing with snow and vegetation. For example, masking of vegetation by snow and vise versa where vegetation masks surface snow with a strong dependence on illumination angle. Another example is snow in mountain regions. For example, assume that almost all the snow existed in shaded areas. If the sky were overcast with only diffuse surface irradiance, mean albedo would be close to a linear weighting based on fractional area of snow and mountain. If the majority of surface irradiance was direct-beam, mean surface albedo would be close to that of the mountain since the snow was in shade. This points to a more general issue: the proper mean albedo to be used in a 1D radiative transfer model is not the areal-weighted mean, but rather the irradiance and areal weighted mean. To do this properly, however, requires a solution for surface irradiance beforehand, which does not exist, and consideration of tilted surfaces. The same then goes for integrations over spectral space: appropriate mean

values require spectral distributions of the quantity being sought! The exact same issue faces computation of broadband atmospheric optical properties.

It is expected that albedo of sea-ice will require increasing attention as representation of sea-ice in LSAMs continues to improve (Kreyscher et al. 2000). It may be that different types of ice can be diagnosed and a μ_0 dependence of albedo assigned to each type. Figure 4 shows an example of the complexity of sea-ice. Surely the roughness characteristics of these surfaces must have an impact on albedo? The same goes for wind-generated sastrugi that exist over vast tracts of Antarctica.

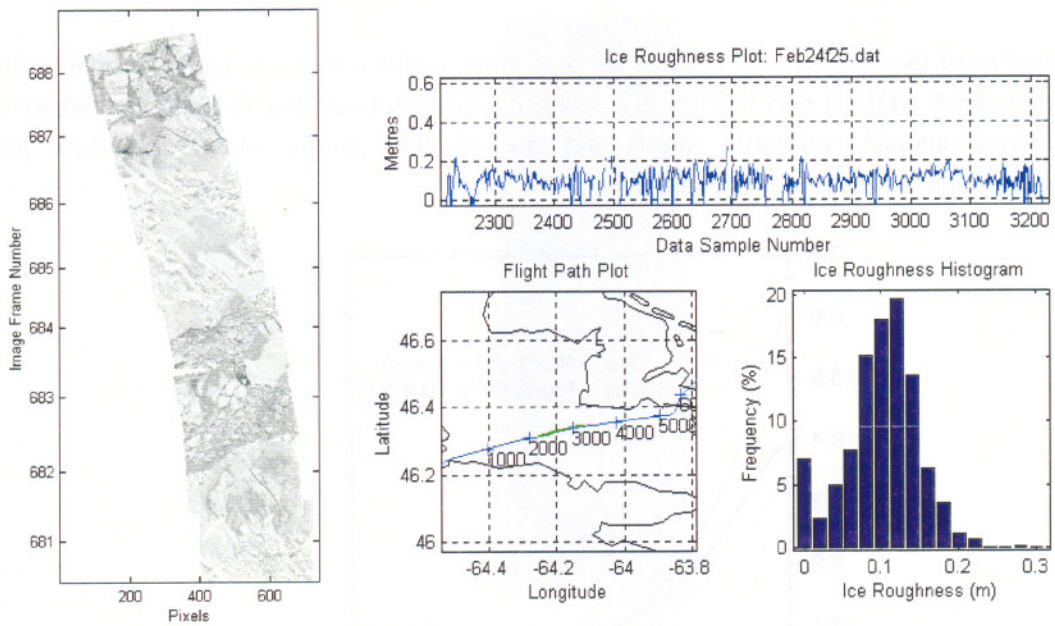

Figure 4. Plot on the left shows imagery of sea-ice in Northhumberland Strait, Canada (image is about 0.5 km wide). Upper plot on the right shows normalized ice altitudes as detected by a helicopter-mounted laser altimeter tracking down the centre of the image on the left. Lower plots on the right show a map of the transect and frequency distribution of ice altitude. (Data courtesy of I. Peterson 2001).

2.4 Clouds

For liquid clouds it is sufficient to assume that droplets are spherical and pure. Cloud optical properties can be computed using Mie theory (e.g., Wiscombe 1980) as functions of refractive indices (e.g., Segelstein 1981), wavelength of radiation, and droplet radius r. Within an LSAM, it is neither efficient nor necessary to perform on-line Mie calculations. Instead, droplet extinction β, ω_0, and g are parametrized as functions of droplet effective radius which is defined as (Hansen and Travis 1974)

$$r_e = \frac{\int_0^\infty r^3 n(r) \mathrm{d}r}{\int_0^\infty r^2 n(r) \mathrm{d}r}, \tag{3}$$

where $n(r)$ is droplet size distribution. The most popular cloud optical property parametrizations for solar wavelengths are those of Slingo (1989) and Hu and Stamnes (1993); both allow up to 24 bands across the solar spectrum. Hu and Stamnes's covers a wider range of r_e than does Slingo's and it also covers the terrestrial spectrum (allowing up to 50 bands). While both parametrizations agree well for β and ω_0, Fig. 5 shows that they disagree considerably for g with Hu and Stamnes in better agreement with Mie values. Having said this, however, Hu and Stamnes's parametrization does exhibit discontinuities at values of r_e where it *skips* from one set coefficients to another.

For clouds consisting of ice, be they mixed phase or entirely ice, specification of optical properties is difficult and questionable. This is because of the many forms that ice crystals can assume (e.g., Liou 1992). The relative rarity of optical phenomena like halos coupled with evidence from particle imaging sensors (Korolev et al. 2001) suggests that, from a climatological standpoint, the habit of most ice crystals is highly irregular. If so, this makes specification of their optical properties for climate studies more tractable (e.g., Macke et al. 1996).

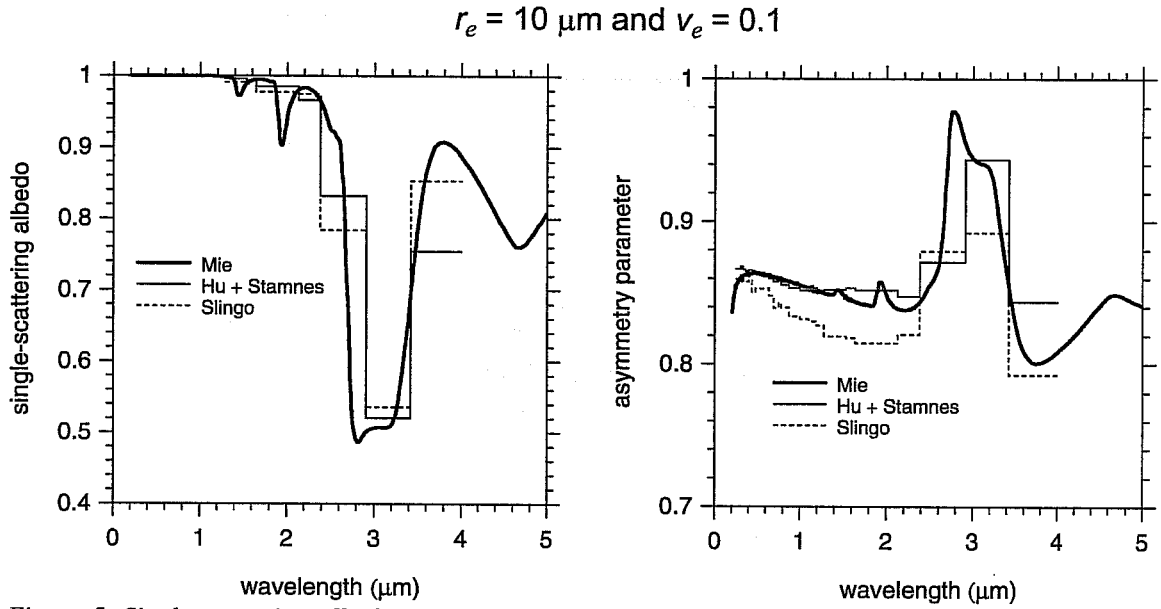

Figure 5. Single-scattering albedo ω0 and asymmetry parameter g predicted by Mie theory for a cloud droplet size distribution described by a gamma distribution with re = 10 μm and effective variance ve = 0.1. Also shown are broadband values of ω0 and g as given by the parametrizations of Hu and Stamnes (1993) and Slingo (1989).

Mixed phase clouds present an added complication. The importance of these clouds is that they absorb more radiation then either mono-phase counterpart as the complex part of the refractive index of liquid and ice are off-set slightly from one another thereby broadening cloud absorption features (Kou et al. 1993). At this stage, the main issue is defining what fraction of the condensed water in an LSAM cell is ice. Aircraft observational studies (Korolev et al. 2000) suggest that this is by no means a straightforward parametrization of temperature as used in many LSAMs. Moreover, the spatial distribution of liquid and ice can be important (Sun and Shine 1994).

Another issue involving mixed phase is precipitation and cloud droplets. Figure 6 shows total water content *TWC*, extinction coefficient β, and droplet effective diameter D_{eff} along two aircraft transects (Korolev et al. 2001). The transect measured on 5/7/83 is simply cloud with no precipitation; changes in β are driven almost

exclusively by changes in *TWC*. For the transect on 2/12/83, however, β is almost constant for the first 15 minutes while *TWC* and D_{eff} vary together. The insensitivity of β to changes in *TWC* suggests the presence of precipitation. It is doubtful whether LSAMs acknowledge the fraction of *TWC* that is precipitation, nor is it clear they need bother for as Fig. 7 shows, *TWC* and β are often correlated well. Where it becomes important, however, is when one tries to either develop or test a cloud water parametrization using aircraft data when the data may contain, at times, large contributions from precipitation.

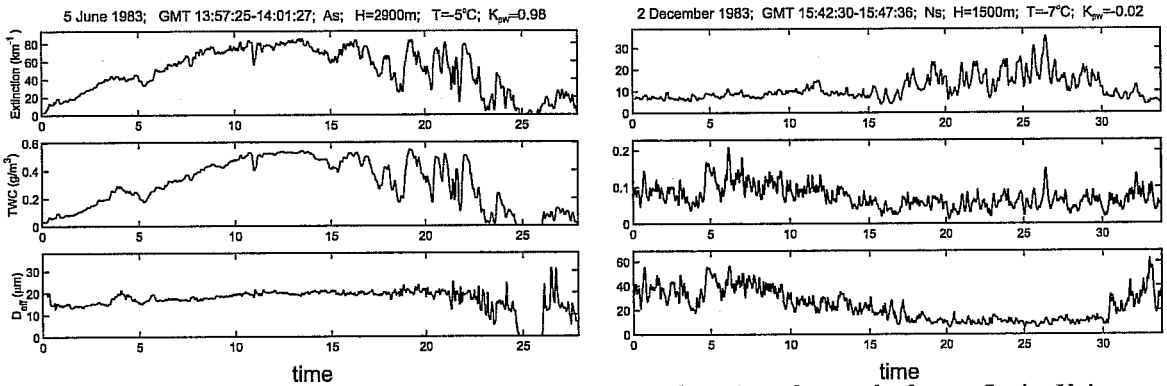

Figure 6. Examples of data collected during two transects of an aircraft over the former Soviet Union. Top panels show visible extinction coefficient (km-1), middle panels show total water content (g m-3), and lower panels show effective diameter of hydrometeors. (Data courtesy of A. Korolev 2001)

3. Radiative transfer

This section focuses on popular techniques of solving the radiative transfer equation for use in multi-layer LSAMs. It contains two main sections; the first is for solar and the second IR radiation. For solar radiation, some results are shown from a recent intercomparison of radiation codes. The focus of the IR section is on a new technique that promises to improve the efficiency of multi-layer IR calculations.

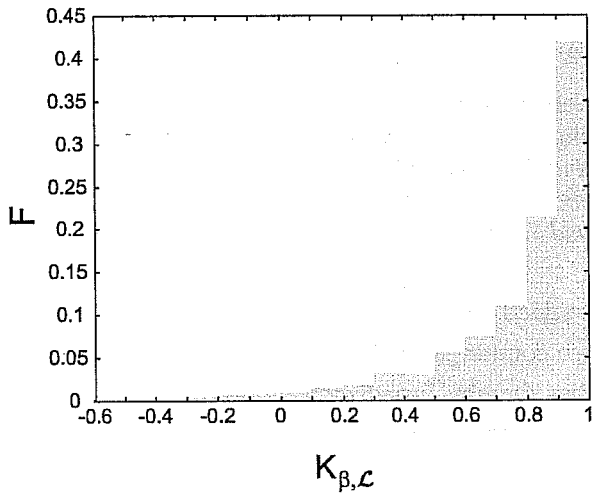

Figure 7. Frequency distribution of correlation between extinction β and total water content L for several thousand 700 m flight legs made over the former Soviet Union. (Data courtesy of A. Korolev 2001).

3.1 Solar radiation

This subsection has three parts. The first discusses two-stream approximations of the radiative transfer equation and computation of layer reflectance and transmittance. The second discusses briefly multi-layer models, and the third presents some results from a recent intercomparison of multi-layer 1D solar codes.

3.1.1 The equation of transfer and two-stream approximations

The steady-state, elastic radiative transfer equation can be written as

$$\mathbf{\Omega}\cdot\nabla I(\mathbf{x},\mathbf{\Omega}) = \sigma(\mathbf{x})I(\mathbf{x},\mathbf{\Omega}) - \sigma_s(\mathbf{x})\int p(\mathbf{\Omega}\cdot\mathbf{\Omega}')I(\mathbf{x},\mathbf{\Omega}')d\mathbf{\Omega}' - f(\mathbf{x},\mathbf{\Omega}), \tag{4}$$

where $\mathbf{x}$ is position, Ω is direction, I is radiance, σ is extinction coefficient, σ_s is scattering coefficient, p is scattering phase function describing the probability of radiation incident from direction Ω being scattered into direction Ω', and f is the attenuated source term. Exact solution of this equation requires an immense amount of information, to make it worth while, and immense computational resources. Solving it in an LSAM is categorically out of the question. Therefore, approximations are required with the intention being computation of reflectance and transmittance for individual model layers.

The first, and most far reaching approximation is

$$\frac{\partial^{\text{optical}}_{\text{properties}}}{\partial x \text{ and } \partial y} = \frac{\partial I}{\partial x} = \frac{\partial I}{\partial y} = 0, \tag{5}$$

which eliminates horizontal fluctuations in both the atmosphere and the radiation field. This simplifies (4) to the 1D equation of transfer that can be written as

$$\mu\frac{dI(\tau,\mu)}{d\tau} = I(\tau,\mu) - \frac{\omega_0}{2}\int_{-1}^{1} p(\mu;\mu')I(\tau,\mu')d\mu' - \frac{F_0}{4}\omega_0 p(\mu;\mu_0)e^{-\tau/\mu_0}, \tag{6}$$

where all terms have been azimuthally averaged, F_0 is incoming solar at the top of atmosphere (TOA), μ is cosine of zenith angle, μ_0 is cosine of solar zenith angle, and

$$d\tau = \sigma ds; \qquad \omega_0 = \sigma_s/\sigma \tag{7}$$

where s is distance, τ is optical thickness, and ω_0 is single-scattering albedo. Defining

$$I^{\pm}(\tau,\mu_0) = \int_0^1 \mu I(\tau,\pm\mu)d\mu, \tag{8}$$

as upwelling and downwelling irradiances, and applying the hemispheric integral operator to (6) yields the coupled equations

$$\begin{cases} \dfrac{dI^-(\tau,\mu_0)}{d\tau} = \gamma_1 I^-(\tau,\mu_0) - \gamma_2 I^+(\tau,\mu_0) - F_0\omega_0\gamma_3 e^{-\tau/\mu_0} \\ \dfrac{dI^+(\tau,\mu_0)}{d\tau} = \gamma_2 I^-(\tau,\mu_0) - \gamma_1 I^+(\tau,\mu_0) + F_0\omega_0\gamma_4 e^{-\tau/\mu_0}, \end{cases} \tag{9}$$

that can be solved readily by standard methods subject to specific boundary conditions where the coefficients $\gamma_1,\ldots\gamma_4$ depend on assumptions made about I and p, as well as on μ_0 and optical properties. Solutions to (9) are referred to as two-stream approximations and are employed by all LSAMs. The general solution to (9) that describes layer reflectance and transmittance for collimated irradiance from above and no upwelling or downwelling diffuse irradiance (Meador and Weaver 1980) is

$$R(\tau,\mu_0) = \frac{\omega_0}{a}\frac{r_+e^{k\tau} - r_-e^{-k\tau} - re^{-\tau/\mu_0}}{e^{k\tau} - \beta e^{-k\tau}}, \tag{10a}$$

and

$$T(\tau,\mu_0) = e^{-\tau/\mu_0}\left\{1 - \frac{\omega_0}{a}\frac{t_+e^{k\tau} - t_-e^{-k\tau} - te^{-\tau/\mu_0}}{e^{k\tau} - \beta e^{-k\tau}}\right\}, \tag{10b}$$

where

$$\begin{aligned} r_\pm &= (1 \mp k\mu_0)(\gamma_1\gamma_3 - \gamma_2\gamma_4 \pm k\gamma_3) \\ t_\pm &= (1 \pm k\mu_0)(\gamma_1\gamma_4 - \gamma_2\gamma_3 \pm k\gamma_4) \\ r &= 2k[\gamma_3 - (\gamma_1\gamma_3 - \gamma_2\gamma_4)\mu_0] \\ t &= 2k[\gamma_4 - (\gamma_1\gamma_4 - \gamma_2\gamma_3)\mu_0] \end{aligned} \tag{10c}$$

and

$$a = \left[1 - (k\mu_0)^2\right](k + \gamma_1)\ ;\ k = \sqrt{\gamma_1^2 - \gamma_2^2},\ ;\ \beta = -\frac{k - \gamma_1}{k + \gamma_1}. \tag{10d}$$

A common assumption made when solving the two-stream involves approximating p as a combination of a smoothly varying portion and a sharp forward scattering peak:

$$p_\delta(\mu,\mu') \equiv 2g^2\delta(\mu - \mu') + (1 - g^2)\left(1 + \frac{3g\mu\mu'}{1+g}\right), \tag{11}$$

where g is asymmetry parameter which equals the mean cosine of scattering angle, and δ is the Dirac function (Joseph et al. 1976). For clouds at least, this approximation is extremely good as can be seen in Fig.8.

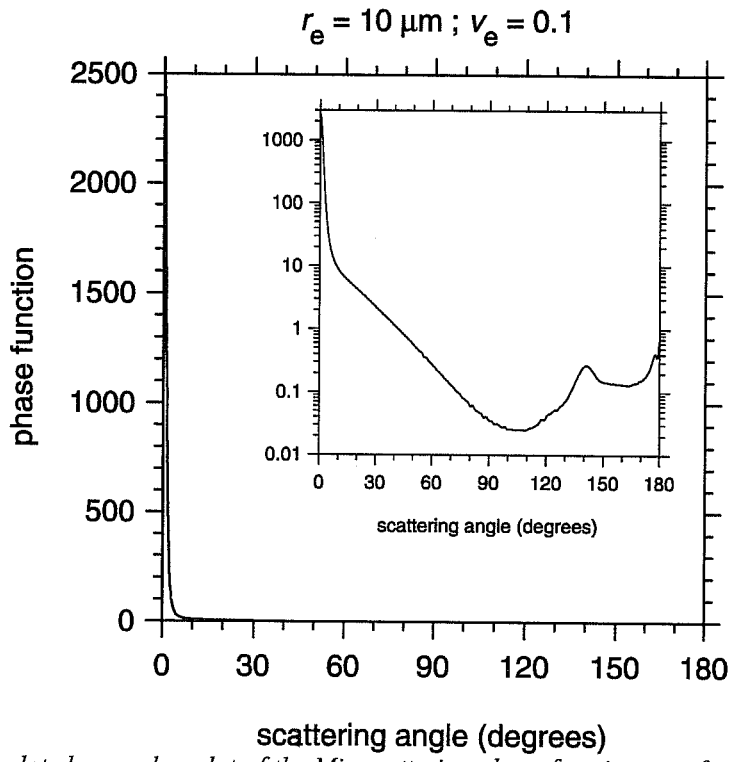

Figure 8. Inset plot shows a log plot of the Mie scattering phase function as a function of scattering angle for a droplet size distribution with re = 10 μm and ve = 0.1 at wavelength 0.6 μm. This is the usual way these functions are presented. The outer plot is the same as the inner except it is on a linear scale. Shown this way it is immediately apparent that the delta function approximation in (10) is perfectly adequate for cloud droplets.

When I is linearized in μ, and substituted along with (11) into (9), it can be shown that (10) results but with the following transformed optical properties:

$$\begin{aligned} \tau' &= (1-\omega_0 g^2)\tau \\ \omega_0' &= \frac{(1-g^2)\omega_0}{(1-\omega_0 g^2)} \\ g' &= \frac{g}{1+g} \end{aligned} \tag{12}$$

Solutions of this type are known as delta-two-streams. While they are generally quite accurate, especially for important high Sun conditions, they tend to scatter too little in near-forward directions and thus, as shown in Fig. 9, lead to systematic underestimates of cloud and aerosol albedo at low Sun. This can be a problem in situations such as Arctic haze where μ_0 is always small yet solar input is large (given long Sun-up periods).

Systematic errors such as these have prompted some (e.g., Qiu 1999; Li 1999a) to concoct parametrizations of g^2 for use in (11). It appears, however, that they are more complicated and computational demanding than necessary.

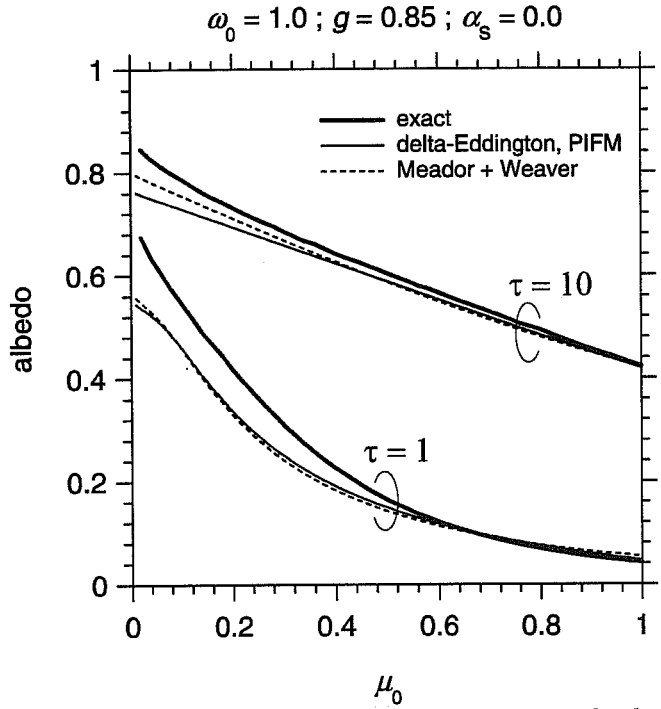

Figure 9. Albedos of single layer, conservative scattering, homogeneous clouds (two optical depth as listed on the plot) as a function of cosine of solar zenith angle using g = 0.85 and a black surface. Heavy solid lines are exact solutions (DISORT), and other lines are two-stream approximations as listed.

Fifteen years ago, King and Harshvardhan (1986) concluded that no single two-stream approximation performs well under all conditions all the time. While this is still true today, it can only be expected given the rather large assumptions behind two-stream approximations. This point is elaborated on later when discussing results from an intercomparison study that involved several solar transfer codes. At the same time, however, it is unlikely that (delta-) two-streams will be replaced as the model of choice in LSAMs. This is because they are computationally inexpensive and given the crude cloud properties they operate on, and will likely operate on in the near future, it makes little sense to replace them with more sophisticated models (e.g., four-streams).

3.1.2 Multi-layer models

One of the key atmospheric conditions governing Earth's radiation budget is cloud fraction A_c. Almost all LSAMs estimate layer A_c, so it is helpful if one's radiative transfer model can incorporate A_c directly. This is achieved best with adding methods. For a simple two-layer system, total reflectance and transmittance are defined as

$$R_{1,2}(\mu_0) = R_1(\mu_0) + \frac{t_1\left\{\left[T_1(\mu_0) - T_1^{dir}\right] r_2 + T_1^{dir} R_2(\mu_0)\right\}}{1 - r_1 r_2}$$

$$T_{1,2}(\mu_0) = T_1^{dir} T_2(\mu_0) + \frac{t_2\left\{\left[T_1(\mu_0) - T_1^{dir}\right] + T_1^{dir} R_2(\mu_0) r_1\right\}}{1 - r_1 r_2} \qquad (13)$$

where the terms are explained schematically in Fig. 10. The geometric sum formula has been applied under the assumption that internal reflections are all equal.

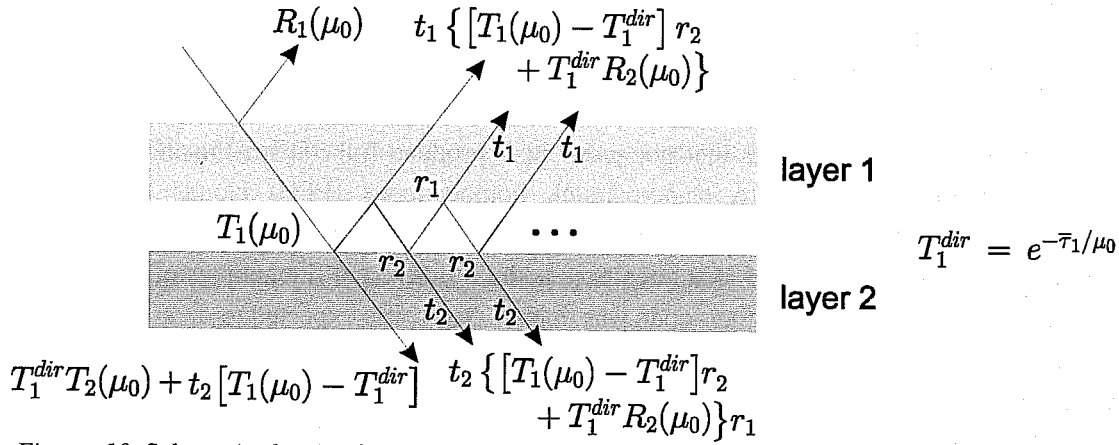

Figure. 10. Schematic showing how layers are linked in a SW adding scheme.

The expressions in (13) can be generalized to any number of layers. Flux profiles are then constructed by working up and down through the atmosphere computing reflectances and transmittances for collections of layers using

$$F_i^{\uparrow} = \mu_0 S \left\{ \frac{T_{1,i-1}^{dir} R_{i,N}(\mu_0) + \left[T_{1,i-1}(\mu_0) - T_{1,i-1}^{dir}\right] r_{i,N}}{1 - r_{i-1,1} r_{i,N}} \right\}$$

$$F_i^{\downarrow} = \mu_0 S \left\{ T_{1,i-1}^{dir} + \frac{T_{1,i-1}^{dir} R_{i,N}(\mu_0) r_{1,i-1} + \left[T_{1,i-1}(\mu_0) - T_{1,i-1}^{dir}\right]}{1 - r_{i-1,1} r_{i,N}} \right\} \tag{14}$$

where the diffuse terms are defined as

$$\begin{aligned} r_{1,2} &= r_1 + \frac{t_1 t_2 r_2}{1 - r_1 r_2} \\ t_{1,2} &= \frac{t_1 t_2}{1 - r_1 r_2} \end{aligned} \tag{15}$$

Expressions like (14) can be computed for both clear and cloudy portions of an atmosphere and linked with adjacent layers depending on the desired nature of vertical overlap of cloud (e.g., Geleyn and Hollingsworth 1979). The most common ways to proceed are to assume random overlap, and to counteract the overestimate of cloud presented to radiation by either reducing cloud fraction or optical thickness, or assume maximum overlap of adjacent layers and random overlap of blocks of layers separated by a cloudless layer(s). The latter approach appears to be becoming the paradigm despite it being an extreme approximation that systematically underestimates total cloud fraction and thus atmospheric reflectance and (most often) heating in clouds (Barker et al. 2002). The next section illustrates the sensitivity of estimated solar fluxes to assumptions about cloud overlap.

3.1.3 Intercomparing 1D and 3D solar transfer codes

To date, the most comprehensive assessment of domain-average, BB irradiances for cloudy atmospheres has been the intercomparison of solar codes by Barker et al. (2002) (see also Barker and Stephens, 2001). The objective of their study was to assess how well 1D codes used in LSAMs interpret and handle unresolved clouds. Several 3D Monte Carlo codes were used to set BB benchmark irradiances. Cloud fields produced by

different cloud-resolving models (CRMs) where used. The Monte Carlos acted on the full fields while 1D codes operated on degenerate versions represented by profiles of A_c, mean cloud optical depth τ, mean logarithm of τ, cloud overlap rate, and mean H_2O vapour mixing ratio.

One of the novelties of this study was that not only did it produce full 3D benchmarks, it also produced *conditional* benchmarks applicable to plane-parallel, homogeneous (PPH) clouds that follow: exact overlapping structure of cloud; maximum overlap; and random overlap. ICA estimates where also given as an appropriate benchmark for 1D codes that attempt to address horizontal fluctuations of unresolved clouds. As such, modellers were able to see if their code was doing what it was expected to do as well as gauge how far their code's performance was from the full 3D solutions. At the same time note that the 3D solutions are not the ultimate truth as an infinite number of 3D domains can give rise to a single set of 1D profiles. The multiplicity of domain-averaged radiative profiles for the allowable 3D fields narrows substantially, however, as the number of 1D profiles increases. For the cases here, the range of possible full 3D solutions is expected to be very narrow. Hence, the 3D results are in all likelihood, excellent representatives of the population they come from.

Before results for complicated cloudy atmospheres can be compared, differences among models for clear-sky and overcast clouds must be established. Unlike the 1D solar code intercomparison study of Fouquart et al. (1991), the current intercomparison study had a better fix on clear and overcast benchmarks. These came from the LBL model CHARTS (Code for High-Resolution Accelerated Radiative Transfer) which has been

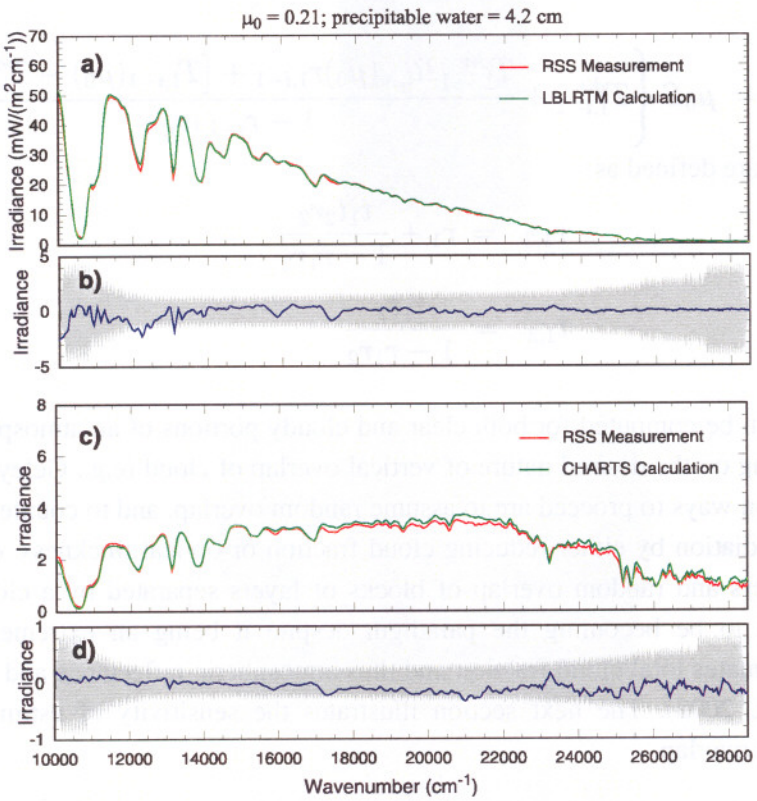

Figure 11. (a) Measured (RSS) and modelled (CHARTS) spectral surface fluxes. Measurements were made on 03/20/2000 at 1226 LST at the Atmospheric Radiation Measurement (ARM) site in OK, USA. Solar zenith angle was 40o, precipitable water amount was 1.16 cm, and assumed aerosol optical depth was 0.0344 (at 0.7 μm; Angstrom exponent of 2.24). (b) Differences between measured and modelled fluxes in (a). (c) and (d) are as in (a) and (b) except they are for corresponding diffuse surface fluxes. (Data courtesy of E. Mlawer 2001).

compared (Mlawer et al. 1999) to high-quality spectral surface irradiance measurements made at the Atmospheric Radiation Measurement Program's Southern Great Plains (ARM-SGP) site (e.g., Stokes and Schwartz 1994). Atmospheric profiles were prescribed based on coincident soundings (cf., Brown et al. 1999). While aerosol optical properties were unknown, values required for CHARTS to yield errors in spectral diffuse irradiance always less than 5% are consistent with recognized aerosol models (Kato et al. 1997). Integrations over wider spectral bands display even smaller errors. Figure 11 shows an example of how well CHARTS performed for a small μ_0 and a heavy water vapour burden.

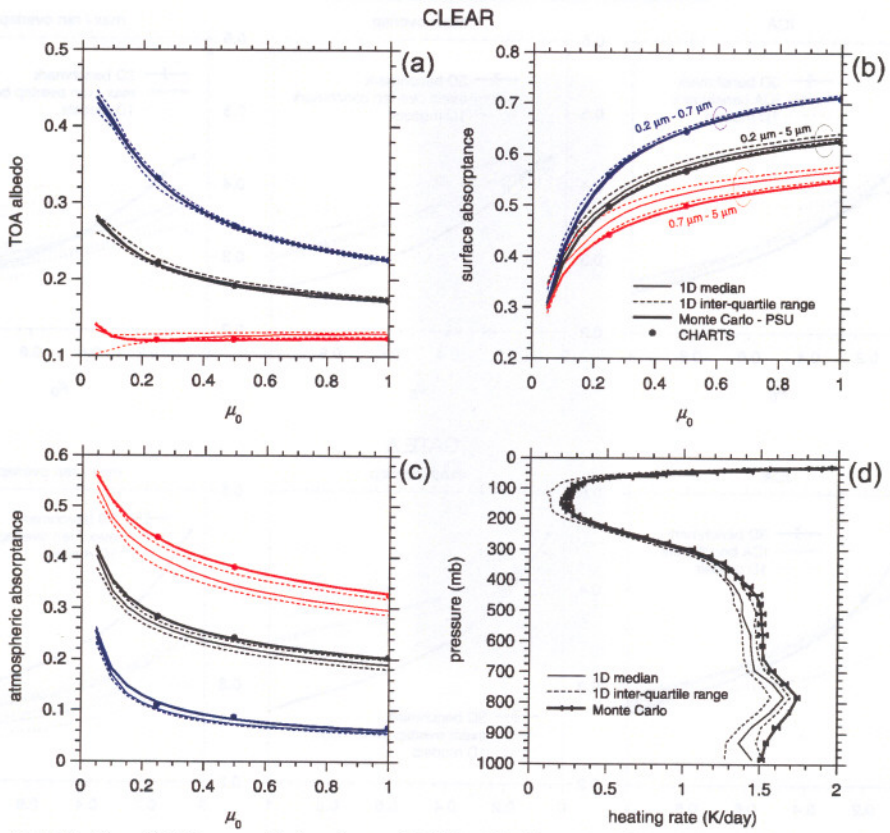

Figure 12. (a) Median (50% quartile) values of TOA albedo αp as functions of μ0 for 1D models for the CLEAR atmosphere for three (colour-coded) spectral ranges as labelled on the plot. Also shown are corresponding 25% and 75% quartiles and benchmark values for a Monte Carlo code and CHARTS. (b) As in (a) except it is for atmospheric absorptance a_{atm}. (c) As in (a) except it is for surface absorptance a_{sfc}. (d) Three quartile values (25%, 50%, and 75%) for 1D model heating rates as a function of pressure at μ0 = 0.5. Also shown is the median value for four 3D MC codes with error bars representing standard deviation.

Figure 13 shows broadband αp as a function of μ0 for two CRM fields (though more were considered in the full report). Each field has three plots that correspond to different treatments of unresolved clouds within 1D codes. Each plot shows 1D model results, respective conditional benchmarks, and means and standard deviations generated by four Monte Carlo codes acting on the full 3D CRM fields. ATEX was a thin boundary layer cloud with domain size (6.8 km)2 and horizontal grid-spacing Δx of 100 m (B. Stevens, per. comm. 1997). GATE A consisted of deep convective clouds (less the cirrus anvil) and was a (400 km) 2 domain with Δx = 2 km (Grabowski et al. 1998).

The 1D codes classed as *ICA* attempt to account for horizontal fluctuations of cloud and possibly overlap (discussed in more detail in the manuscript entitled *Radiative Transfer and Cloud Variability: From Remote Sensing to Climate Sensitivity* in this volume). As Fig. 13 shows, these 1D codes can track the *ICA* and full 3D benchmarks well. The 1D codes classed as *exact overlap* attempt to overlap PPH clouds in manners resembling the CRM fields. Note that the *exact overlap* benchmark is almost always more reflective than the full 3D and always more reflective than the *ICA* benchmarks. The 1D codes of this genre tend to be *attracted* to their conditional benchmark though variance is large; especially for GATE A where these codes were subject to a particularly demanding test.

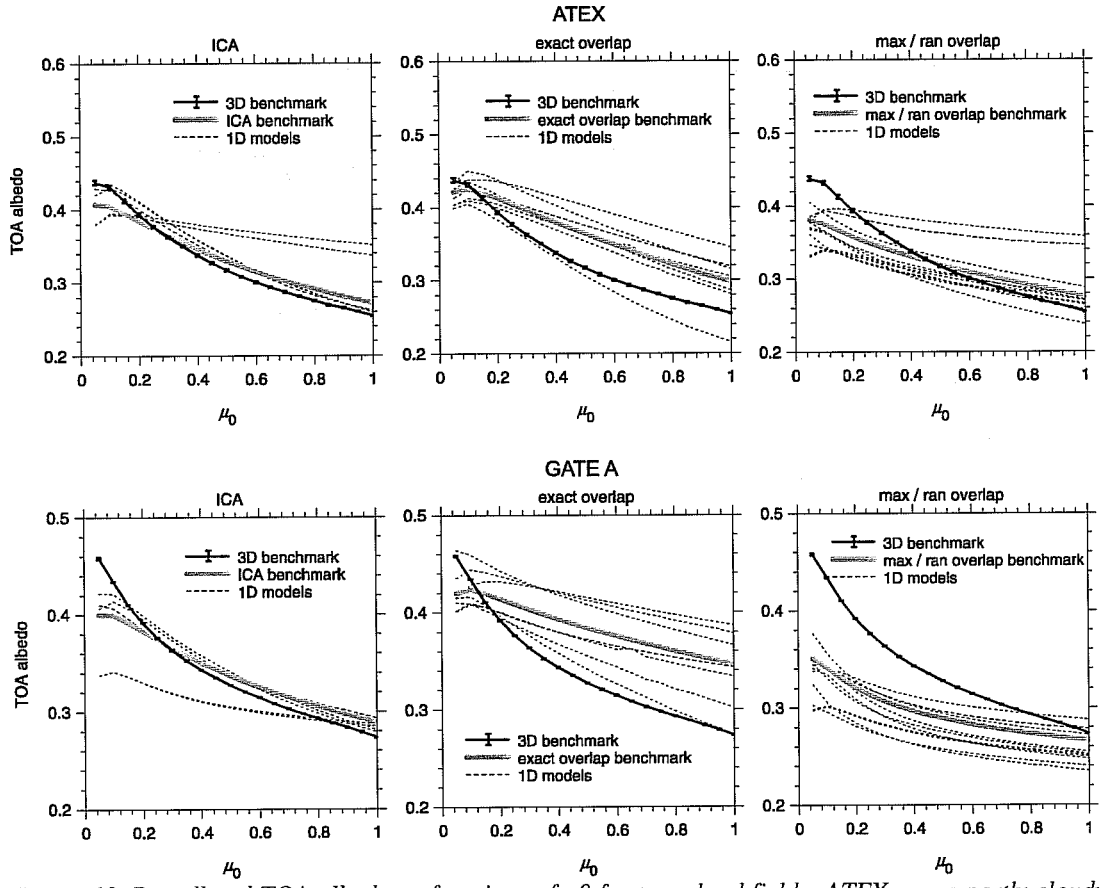

Figure 13. Broadband TOA albedo as functions of μ0 for two cloud fields; ATEX was a partly cloudy stratocumulus and GATE A was a deep tropical convective system. Solid black lines are the means of four Monte Carlo codes operating on the full 3D variability; errors bars represent standard deviations. These values represent the ultimate benchmarks. Heavy gray lines are conditional benchmarks (as indicated in the title on the plots) produced by one of the Monte Carlos. Dashed lines are 1D model results. The 1D codes were sorted into categories according to how they handle unresolved clouds (see text for discussion).

Maximum/random overlap is the most populated category. Benchmark estimates of αp for this genre are always less than those for *exact overlap* due to less cloud exposed to radiation. Often they are even less reflective than *ICA* and full 3D; this attests to it being an extreme approximation that can radically underestimate total cloud fraction. Nevertheless, corresponding 1D codes tend to follow, though almost always underestimate, their conditional benchmark. It should be noted that if codes in this class were to include the effects of unresolved horizontal variability (as did those in the *ICA* category), their estimates of αp would be even smaller than shown here.

3.2 Infrared radiation

Historically, infrared radiative transfer calculations have required excessive shares of an LSAM's execution time (often over 30% of the entire model!). This even when scattering is neglected. At the expense of going over traditional methods of performing IR transfer calculations, a new approach developed recently by Li (2002) will be presented briefly. Li's method requires significantly less CPU time than traditional methods, yet is just as accurate and includes scattering, generalized overlap, and unresolved cloud effects (as explained in the companion paper to this one).

The IR counterpart to (6) can be expressed as

$$\mu \frac{dI(\tau,\mu)}{d\tau} = I(\tau,\mu) - \frac{\omega_0}{2}\int_{-1}^{1} p(\mu;\mu')I(\tau,\mu')d\mu' - (1-\omega_0)\,B(T) \tag{16}$$

where $B(T)$ is the Planck function at temperature T. Assuming the absorption approximation in conjunction with a pure Dirac phase function, (16) becomes

$$\mu \frac{dI(\tau,\mu)}{d\tau} = (1-\omega_0)\,I(\tau,\mu) - (1-\omega_0)\,B(T). \tag{17}$$

Assuming an isothermal layer, the solution to (17) for downwelling flux at the base of the jth layer, for example, is

$$F^{-}_{j+1} = F^{-}_{j} e^{-\langle\kappa\rangle_j/\mu_1} + B'_{j+\frac{1}{2}}\left(1 - e^{-\langle\kappa\rangle_j/\mu_1}\right) \tag{18}$$

where $\mu_1 = 0.601$ (Li 1999b), $B' = \pi B$, and

$$\langle\kappa\rangle_j = (1-\omega_0)\,\tau_j \tag{19}$$

is absorption optical depth for the jth layer. In a similar manner to (14), flux profiles can be built by working (18) up and down through the atmosphere. As such, the need to compute explicit contributions for all combinations of layers (i.e., the traditional approach) is alleviated and the number of IR computations scale directly with the number of layers (not the square of the number of layers as in traditional schemes).

When considering overlap of cloud with this scheme, mean fluxes emerging from a layer are defined as

$$F^{-}_{i+1} = (1-c_i)\mathcal{M}^{-}_{i+1} + c_i\mathcal{N}^{-}_{i+1}, \tag{20}$$

where c_i is cloud fraction in the ith layer and

$$\mathcal{M}^-_{i+2} = \left[\frac{\overset{①}{(c_i - o_{i,i+1})\mathcal{N}^-_{i+1}} + \overset{②}{(1 - c_i - c_{i+1} + o_{i,i+1})\mathcal{M}^-_{i+1}}}{1 - c_{i+1}} - B'_{i+1+\frac{1}{2}}\right] e^{-\tau_{i+1}/\mu_1} + B'_{i+1+\frac{1}{2}}$$

$$\mathcal{N}^-_{i+2} = \left[\frac{\overset{③}{o_{i,i+1}\mathcal{N}^-_{i+1}} + \overset{④}{(c_{i+1} - o_{i,i+1})\mathcal{M}^-_{i+1}}}{c_{i+1}} - B'_{i+1+\frac{1}{2}}\right] e^{-\langle\kappa\rangle_{i+1}/\mu_1} + B'_{i+1+\frac{1}{2}} \tag{21}$$

are the clear and cloudy contributions, respectively, where the numerated terms in (21) are illustrated graphically in Fig. 14, and $o_{i,i+1}$ is the overlapping fraction of clouds in adjacent layers.

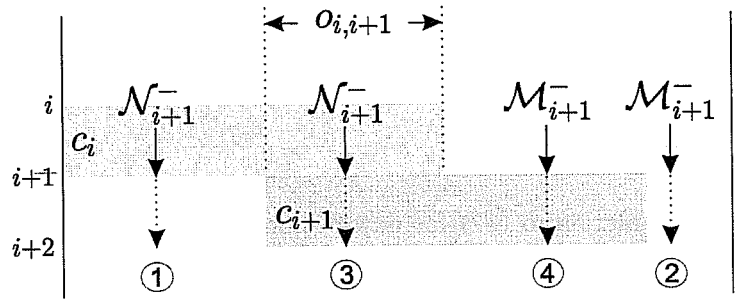

Figure. 14. Schematic showing how Li's (2002) multi-layer LW scheme handles overlapping clouds. See Eq. (21).

Scattering can be approximated easily with this method using a perturbation method (Li 2002). Instead of using (18) to compute downwelling flux, it is computed as

$$F^+_j = \underbrace{F^+_{j+1}e^{-\langle\kappa\rangle_j/\mu_1} + \tilde{B}_{j+\frac{1}{2}}\left(1 - e^{-\langle\kappa\rangle_j/\mu_1}\right)}_{\text{AA } (0^{th} - \text{order scattering})} + S^+_j, \tag{22}$$

where

$$S^+_j = -\frac{\omega_0}{2(1-\omega_0)}\left(1 - 3\mu_1^2\right)\left[\frac{\langle\kappa\rangle_j}{\mu_1}e^{-\langle\kappa\rangle_j/\mu_1}\left(F^{(0)}_{j+1} - \tilde{B}_{j+\frac{1}{2}}\right) + \frac{1}{2}\left(e^{-2\langle\kappa\rangle_j/\mu_1} - 1\right)\left(F^{(0)}_j - \tilde{B}_{j+\frac{1}{2}}\right)\right], \tag{23}$$

in which $F_j^{(0)}$ is obtained from the absorption approximation (Eq. 18). Application of this term to downwelling fluxes only yields errors that are typically less than 1 W m^{-2} (Li 2002).

Figure 15 shows how well the code just described can perform when compared to an independent column approximation (ICA). The ICA values were computed by averaging results from several columns using the same code with cells that were either overcast or clear. These are stringent cases that rigorously test the

ability of the single column code to handle virtually all overlap conditions. The only case that presents major difficulty is case D.

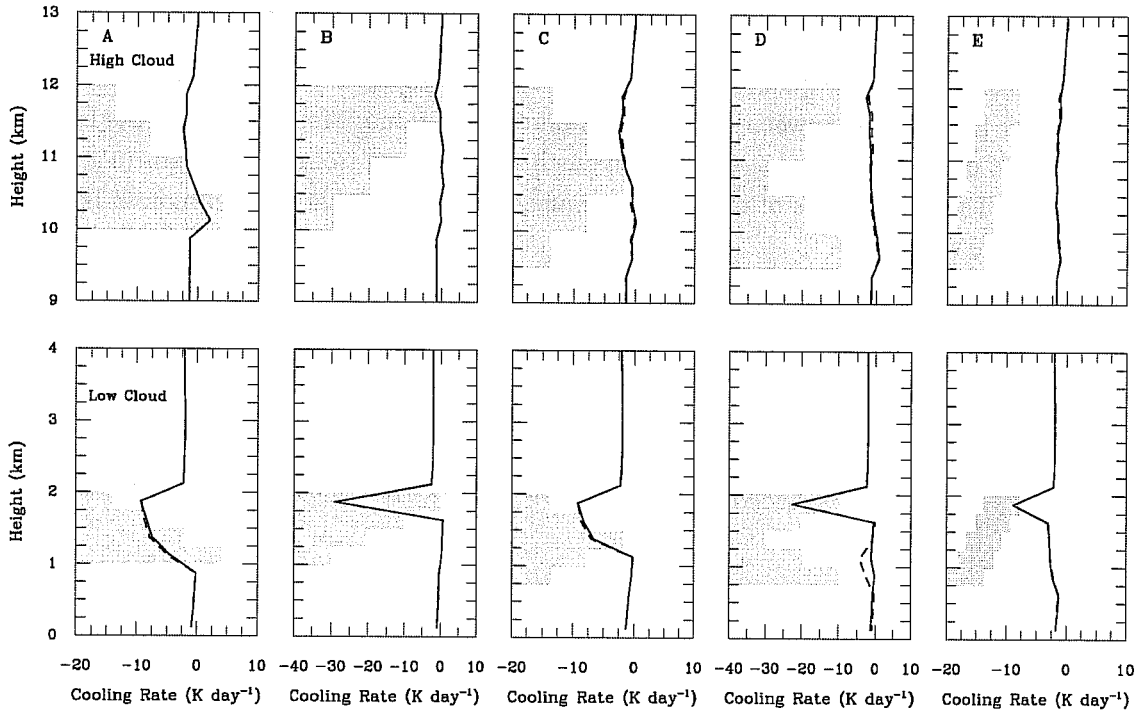

Figure 15. Shaded areas indicate the location and fractional amount of contiguous layered high (ice) and low (liquid) clouds. Solid lines are heating rates from the ICA estimate and represent the benchmarks; dashed lines are from Li's (2002) 1D algorithm.

4. Conclusion

The purpose of this manuscript was to provide a brief overview of some issues facing computation of broadband radiative fluxes within LSAMs. It was not intended to be an exhaustive review. Moreover, issues that were either neglected entirely or mentioned in passing, and there were many, should not be viewed as either trivial, unworthy, or solved entirely. It is hoped, however, that the main points discussed here represent interesting issues that face modelling of radiative transfer and optical properties in LSAMs. This includes perhaps some unexpected elaborations on matters such as surface albedo, intercomparing 1D codes, and a novel means of computing IR transfer.

To summarize, computation of gaseous transmittances was discussed briefly for it is felt that the community is entrenched rather firmly in the CKD paradigm; and justifiably so given the wealth of work, accuracy, and efficiency this methodology brings (at this point). At the same time, it was shown that LBL models appear to be yielding what many would consider to be very reliable benchmarks. This stems from accurate spectral information and modelling, and high quality radiometric measurements.

Regarding aerosol and cloud optical properties, clearly work still remains to be done. Especially in the areas of aerosol characterization and chemistry, parametrization of broadband cloud optical properties, and mixed phase issues. Though not discussed, cloud fraction is perhaps the single most important cloud-radiation

parameter, yet at the same time it maybe the most ill-defined, over-worked property. This is so because it is far from clear that cloud fractions produced by the cloud routine of an LSAMs are those used by, or intended to be used by, corresponding radiation routines. Nor is it clear that cloud fractions reported by cloud atlases are those that LSAMs want to compare to. Nevertheless, recent studies (e.g., Xu and Randall 1996) that have attempted a bottom-up approach to parametrization of cloud fraction likely point the way for future research.

The outstanding challenges for radiation transfer in LSAMs seem then to be those associated with parametrization of interactions between radiation and unresolved cloud. Most of the work is likely to be in parametrizations of unresolved cloud structure with much work coming from observations (e.g., Hogan and Illingworth 2000). This is the focus of this paper's companion that deals, in part, with these issues for both short- and long-wave radiation.

References

Arking, A. and K. Grossman, 1972: The influence of of line shape and band structure on temperatures in planetary atmospheres. J. Atmos. Sci., 29, 937-949.

Arking, A., 1999: Bring climate models into agreement with observations of atmospheric absorption. J. Climate, 12, 1589-1600.

Barker, H. W., 1995: Reassessing the elliptic phase function for use in two-stream approximations. J. Atmos. Sci., 52, 2227-2231.

Barker, H.W. and Z. Li, 1995: Improved simulation of clear-sky solar radiative transfer in the CCC-GCM. J. Climate, 8, 2213- 2223.

Barker, H. W., G. L. Stephens, and Q. Fu, 1999: The sensitivity of domain-averaged solar fluxes to assumptions about cloud geometry. Q. J. R. Meteorol. Soc., 125, 2127-2152.

Barker, H. W. and G. L. Stephens, 2001: An Intercomparison of 1D Solar Radiative Transfer Codes: From Simple to Complex Cloudy Atmospheres. GEWEX Newsletter, 11, 7-10.

Barker, H. W., G. L. Stephens, P. T. Partain and 29 others, 2002: Assessing 1D Atmospheric Solar Radiative Transfer Models: Interpretation and Handling of Unresolved Clouds. Submitted to J. Geophys. Res.

Blanchet, J.-P., 1982: Application of the Chandrasekhar mean to aerosol optical parameters. Atmos. Ocean, 10, 189-206.

Briegleb, B. P., P. Minnis, V. Ramanathan, and E. Harrison, 1986: Comparison of regional clear-sky albedos inferred from satellite observations and model computations. J. Clim. and Appl. Meteor., 25, 214-226.

Brown, P. D., S. A. Clough, E. J. Mlawer, T. R. Shippert, and F. J. Murcray, 1999: High resolution validation in the shortwave: ASTI/LBLRTM QME. Proceedings of the Eighth Atmospheric Radiation Measurement (ARM) Science Team Meeting, DOE/ER-0738, pp. 101-108, U.S. Department of Energy.

Chylek, P., J. T. Kiehl, and M. K. W. Ko, 1978: Narrow resonance structure in the Mie scattering characteristics, Appl. Opt. 17, 3019-3021.

Clough, S. A., F. X. Kneizys, and R. W. Davies, 1989: Line shape and the water vapor continuum. Atmos. Res., 23, 229-241.

Coakley, J. A., Jr., and P. Chylek, 1975: The two-stream approximation in radiative transfer: Including the angle of the incident radiation. J. Atmos. Sci., 32, 409-418.

Coakley, J. A., Jr., and R. D. Cess, 1985: Response of the NCAR community climate model to the radiative forcing of the naturally occurring tropospheric aerosol. J. Atmos. Sci., 42, 1677-1692.

Cox, C. and W. Munk, 1956: Slopes of the sea surface deduced from photographs of the sun glitter. Bull. Scripps Inst. Oceanog., 6, 401-488.

ESA, 2001: The Five Candidate Earth Explorer Core Missions: Reports for Assessment. SP-1257-5.

Fouquart, Y. and B. Bonnel, 1980: Computations of solar heating of the Earth's atmosphere: A new parameterization. Cont. Atmos. Phys., 53, 35-62.

Fouquart, Y., B. Bonnel, and V. Ramaswamy, 1991: Intercomparing shortwave radiation codes for climate studies. J. Geophys. Res., 96, 8955-8968.

Fu, Q. and K.-N. Liou, 1992: On the correlated-k distribution method for radiative transfer in inhomogeneous atmospheres. J. Atmos. Sci., 49, 2139-2156.

Geleyn, J. -F. and A. Hollingsworth, 1979: An economical analytical method for the computation of the interaction between scattering and line absorption of radiation. Cont. Atmos. Phys., 52, 1-16.

Grabowski, W. W., X. Wu, M. W. Moncrieff, and W. D. Hall, 1998: Cloud-resolving modeling of cloud systems during phase III of GATE. Part II: Effects of resolution and the third spatial dimension. J. Atmos. Sci., 55, 3264-3282.

Hansen, J. E. and L. D. Travis, 1974: Light scattering in planetary atmospheres. Space Sci. Rev., 16, 527-610.

Hansen, J. E., D. Russell, D. Rind, P. Stone, A. Lacis, L. Travis, S. Lebedeff, and R. Ruedy, 1983: Efficient three-dimensional global models for climate studies: Models I and II. Mon. Wea. Rev., 111, 609-662.

Henyey, L. C. and J. L. Greenstein, 1941: Diffuse radiation in the galaxy. Astrophys. J., 93, 70-83.

Hogan, R. J. and A. J. Illingworth, 2000: Derived cloud overlap statistics from radar. Q. J. R. Meteorol. Soc., 126, 2903-2909.

Hu, Y. X. and K. Stamnes, 1993: An accurate parameterization of the radiative properties of water clouds suitable for use in climate models. J. Climate, 6, 728-742.

Joseph, J. H., W. J. Wiscombe, and J. A. Weinman, 1976: The delta-Eddington approximation for radiative transfer. J. Atmos. Sci., 33, 2452-2459.

Kato, S., T. P. Ackerman, E. E. Clothiaux, J. H. Mather, G. G. Mace, M. L. Wesley, F. Murcray, and J. Michalsky, 1997: Uncertainties in modeled and measured clear-sky surface shortwave irradiances. J. Geophys. Res., 102, 25,881-25,898.

King, M.D., and Harshvardhan, 1986: Comparative accuracy of selected multiple scattering approximations, J. Atmos. Sci., 43, 784-801.

Korolev, A. V., G. A. Isaac, and J. Hallett, 2000: Ice particle habits in stratiform clouds. Q. J. R. Meteorol. Soc.,126, 2873-2902.

Korolev, A. V., G. A. Isaac, I. P. Mazin, and H. W. Barker, 2001: Microphysical properties of continental stratiform clouds. In press Q. J. R. Meteorol. Soc.

Kou, L. D. Labrie, and P. Chylek: 1993: Refractive indices of water and ice in the 0.65-2.5 □m spectral range. Appl. Opt., 33, 3531-3540.

Kreyscher, M., M. Harder, P. Lemke and G. M. Flato, 2000: Results of the Sea Ice Model Intercomparison Project: Evaluatoin of sea-ice rheology schemes for use in climate simulations. J. Geophys. Res., 105, 11299 - 11320.

Lacis, A. A. and V. Oinas, 1991: A description of the correlated-k method for modeling nongrey gaseous absorption, thermal emission, and multiple scattering in vertically inhomogeneous atmospheres. J. Geophys. Res., 96, 9027-9063.

Lacis, A. A., W. C. Wang, and J. E. Hansen, 1979: Correlated-k method for radiative transfer in climate models: Application to the effect of cirrus clouds on climate. NASA Conf. Publ. 2076, 309-314.

Li, J., 1999a: On the Fractional Scattering into the Forward Peak. J. Atmos. Sci., 56, 2728-2732.

Li, J., 1999b: Gaussian quadrature and its application to infrared radiation. J. Atmos. Sci., 56, 753-765.

Li, J., J. G. Wong, D., J. S. Dobbie, and P. Chylek, 2001: Parameterization of the optical properties and growth of sulfate aerosols. J. Atmos. Sci., 58, 193-209.

Li., J., 2002: Accounting for unresolved clouds in a 1D infrared radiative transfer model. Part I: Solution for radiative transfer, scattering, and cloud overlap. In press J. Atmos. Sci.

Liou, K. -N., 1992: Radiation and cloud processes in the atmosphere. Oxford University Press, New York, 487pp.

Macke, A., J. Mueller, and E. Raschke, 1996: Single scattering properties of atmospheric ice crystals. J. Atmos. Sci., 53, 2813-2825.

Meador, W. E. and W. R. Weaver, 1980: Two-stream approximations to radiative transfer in planetary atmospheres: A unified description of existing methods and a new improvement. J. Atmos. Sci., 37, 630-643.

Mlawer, E. J., P. D. Brown, S. A. Clough, L. C. Harrison, J. J. Michalsky, P. W. Kiedron, and T. Shippert, 2000: Comparison of spectral direct and diffuse solar irradiance measurements and calculations for cloud-free conditions. In press Geophys. Res. Lett.

Monahan, E. C. and I. G. O'Muircheartaigh, 1987: Comments on "Albedos and glitter patterns of a wind-roughened sea surface". J. Phy. Oceanogr., 17, 549-550.

Payne, R. E., 1972: Albedo of the sea surface. J. Atmos. Sci., 29, 959-970.

Preisendorfer, R. W. and C. D. Mobley, 1986: Albedos and glitter patterns of a wind-roughened sea surface. J. Phy. Oceanogr., 16, 1293-1316.

Qiu, J., 1999: Modified Delta-Eddington Approximation for Solar Reflection, Transmission, and Absorption Calculations. J. Atmos. Sci., 56, 2955-2961.

Ramaswamy, V. and S. Freidenreich, 1991: Solar radiative line-by-line determination of water vapor absorption and water cloud extinction in inhomogeneous atmospheres. J. Geophys. Res., 96, 9133-9157.

Segelstein, D., 1981: The Complex Refractive Index of Water. M.S. Thesis, University of Missouri-Kansas City.

Slingo, A., 1989: A GCM parameterization for the shortwave radiative properties of water clouds. J. Atmos. Sci., 46, 1419-1427.

Stephens, G.L. and S.-C. Tsay, 1990: On the cloud absorption anomaly Q. J. R. Meteorol. Soc., 116, 671-704.

Stokes, G. M., and S. E. Schwartz, 1994: The atmospheric radiation measurement (ARM) program: Programmatic background and design of the cloud and radiation test bed. Bull. Amer. Meteor. Soc., 75, 1201-1221.

Sun, Z. and K. P. Shine, 1994: Studies of the radiative properties of ice and mixed-phase clouds. Q. J. R. Meteorol. Soc., 120, 111-137.

Wiscombe, W. J. and J. W. Evans, 1976: Exponential-sum fitting of radiative transmission functions. J. Comp. Phys., 24, 416-444.

Wiscombe, W. J., 1980: Improved Mie Scattering Algorithms. Appl. Opt., 19, 1505-1509.

Xu, K.-M. and D. A. Randall, 1996: A semiempirical cloudiness parameterization for use in climate models. J. Atmos. Sci., 53, 3084-3102.